Quantitative Imaging of Lateral ErbB1 Receptor Signal Propagation in the Plasma Membrane

Peter J. Verveer, *et al.*

Science **290**, 1567 (2000);
DOI: 10.1126/science.290.5496.1567

15. T. E. Tullis, J. Tullis, in *Mineral and Rock Deformation; Laboratory Studies; The Paterson Volume*, B. E. Hobbs, H. C. Heard, Eds. (American Geophysical Union, Washington, DC, 1986), vol. 36, pp. 297–324.
16. Samples were prepared as follows: Optically transparent single crystals of San Carlos olivine $(Mg_{0.906}Fe_{0.091}Ni_{0.003})_2SiO_4$ were crushed with a tempered steel piston and were ground using an agate pestle and mortar. The material was dry-sieved, resulting in powders with 15- to 32-μm grain sizes. Samples were cold-pressed in an iron jacket under uniaxial stress (~150 MPa). Powders and cold presses were stored at 150°C in a 1-bar oven. Cold-pressed samples were isostatically hot-pressed in an internally heated gas medium vessel at 1200°C and 300MPa confining pressure for 12 hours, and were immediately deformed.
17. M. S. Paterson, D. L. Olgaard, *J. Struct. Geol.* **22**, 1341 (2000).
18. Web figure 1 illustrating the sample assembly is available at *Science* Online at www.sciencemag.org/cgi/content/full/290/5496/1564/DC1.
19. Rheological parameters in torsion experiments were obtained as follows: Shear strain γ at a given position in the sample is proportional to twist angle θ and radial distance from cylinder axis. The same holds true for rates $\dot{\gamma}$ and $\dot{\theta}$. Most of the applied torque M is supported by the outer rim of the specimen. For a homogeneous isotropic material, the shear stress τ is proportional to M, assuming a uniform power law rheology $\dot{\gamma} \propto \tau^n$ with a constant stress exponent n throughout the sample. A related power law $\dot{\theta} \propto M^n$ holds with the same exponent n (*17, 30, 31*). Stepping tests (where M is measured as a function of $\dot{\theta}$) allow n to be determined at different total shear strains γ.
20. Infrared spectra were measured by S. Mackwell at the Bayerisches Geoinstitut, Universität Bayreuth.
21. A. M. Boullier, A. Nicolas, *Phys. Chem. Earth* **9**, 467 (1975).
22. A. Tommasi, B. Tikoff, A. Vauchez, *Earth Planet. Sci. Lett.* **168**, 173 (1999).
23. H. R. Wenk, C. N. Tomé, *J. Geophys. Res.* **104**, 25513 (1999).
24. A. Nicolas, *Rev. Geophys* **24**, 875 (1986).
25. S. Karato, P. Wu, *Science* **260**, 771 (1993).
26. B. Wernicke, B. C. Burchfiel, *J. Struct. Geol.* **4(2)**, 105 (1982).
27. G. Boillot, G. Feraud, M. Recq, J. Girardeau, *Nature* **341**, 523 (1989).
28. F. A. Cook, A. J. van der Velden, K. W. Hall, B. J. Roberts, *Geology* **26**, 839 (1998).
29. ———, *Tectonics* **18**, 1 (1999).
30. G. R. Canova, S. Shrivastava, J. J. Jonas, C. G'Sell, in *Symposium on Formability of Metallic Materials—2000 A.D.*, J. R. Newby, B. A. Niemeier, Eds., Chicago, IL, 24 to 25 June 1980 (American Society for Testing and Materials special publication 753, Chicago, 1982), pp. 189–210.
31. J. A. Bailey, in *Metals Handbook, Vol. 8 Mechanical Testing* (American Society for Metals, Metals Park, OH, 1985), pp 139–144.
32. H. R. Wenk, S. Matthies, J. Donovan, D. Chateigner, *J. App. Cryst.* **31**, 262 (1998).
33. D. Mainprice, *Comput. Geosci.* **16**, 385 (1990).
34. We thank M. Paterson for the design and installation of the torsion apparatus, S. Mackwell for FTIR measurements and for stimulating discussions, M. Schmocker and A. Barnhoorn for assistance, R. Hofmann for workshop support, R. Wessicken for SEM maintenance, and F. Pirovino for thin section preparations. We also gratefully acknowledge two anonymous referees for providing constructive reviews. Supported by the Swiss Nationalfond No. 2000-052494.97/1.

18 July 2000; accepted 10 October 2000

Quantitative Imaging of Lateral ErbB1 Receptor Signal Propagation in the Plasma Membrane

Peter J. Verveer,[1]* Fred S. Wouters,[1]* Andrew R. Reynolds,[2]* Philippe I. H. Bastiaens[1,2]†

Evidence for a new signaling mechanism consisting of ligand-independent lateral propagation of receptor activation in the plasma membrane is presented. We visualized the phosphorylation of green fluorescent protein (GFP)–tagged ErbB1 (ErbB1-GFP) receptors in cells focally stimulated with epidermal growth factor (EGF) covalently attached to beads. This was achieved by quantitative imaging of protein reaction states in cells by fluorescence resonance energy transfer (FRET) with global analysis of fluorescence lifetime imaging microscopy (FLIM) data. The rapid and extensive propagation of receptor phosphorylation over the entire cell after focal stimulation demonstrates a signaling wave at the plasma membrane resulting in full activation of all receptors.

Ligand-driven ErbB1 activation is generally thought to occur through the formation of stable receptor dimers (*1–5*). The proximity of the two ErbB1 receptors in the stable dimer allows subsequent transactivation by cross-phosphorylation of target tyrosine residues by the receptor tyrosine kinase domain, both located in the cytoplasmic tail of the receptor (*6*, *7*). Signal transduction then proceeds through recruitment to the receptors of phosphotyrosine-binding adaptor and effector proteins, such as Grb2, SHC, and p85 (*8–10*). We provide evidence for a different ErbB1 signaling mechanism of ligand-independent lateral propagation of receptor activation in the plasma membrane where the activated receptor dimer is a transient rather than a stable feature. To show this, we induced local activation of ErbB1-GFP by applying EGF covalently attached to beads (EGF-beads) and monitored the phosphorylation state of the receptors across the whole cell. The extent of ErbB1 receptor phosphorylation was mapped by measuring FRET between ErbB1-GFP and a Cy3-labeled antibody to phosphotyrosine (Cy3/PY72).

The occurrence of FRET causes the fluorescence lifetime of the phosphorylated receptor to decrease (*11–13*), which is detected using FLIM (*14–17*). Efficient FRET will occur only when the Cy3 acceptor is brought within nanometer range of the GFP donor by binding of the antibody to the phosphorylated receptor (*11*). A global FLIM analysis technique was developed (*18*) that uses the understanding that the receptor exists in two states, phosphorylated or unphosphorylated, each with a unique associated fluorescence lifetime (Fig. 1A). As a result, quantitative maps of the populations of each state are obtained (Fig. 1B). In addition, the lifetime of each state is determined, from which the true FRET efficiency in the receptor-antibody complex can be calculated. This approach allows quantitative and precise mapping of the relative concentration of phosphorylated protein in cells, whereas earlier approaches were qualitative (*12*, *19*).

To study the lateral propagation of ErbB1-GFP phosphorylation, the population distribution of phosphorylated receptors in cells after focal stimulation with 0.8-μm diameter EGF-beads (*20*, *21*) was compared with the distribution after exposure to a saturating dose (0.1 μg/ml) of soluble EGF. Groups of MCF7 cells expressing ErbB1-GFP were microinjected with Cy3-labeled Fab fragments (*22*) of a phosphotyrosine-specific antibody (Cy3/FabPY72) and stimulated. Average ErbB1-GFP expression levels in MCF7 cells (5×10^5) were half that of A431 cells, as judged by the fluorescence intensity of receptor-bound Cy3-EGF. Cells treated with soluble EGF showed a homogeneous phosphorylation pattern at the plasma membrane that was maximal 15 min after stimulation (Fig. 2A). Cells stimulated with EGF-beads (red dots, Fig. 2A) also exhibited an extended phosphorylation pattern, to the same extent as found after stimulation with soluble EGF, indicative of extensive lateral spreading of ErbB1 phosphorylation.

In these experiments, the kinetics of anti-

[1]Cell Biology and Cell Biophysics Program, European Molecular Biology Laboratory, Meyerhofstrasse 1, 69117 Heidelberg, Germany. [2]Cell Biophysics Laboratory, Imperial Cancer Research Fund, 44 Lincoln's Inn Fields, London, WC2A 3PX, UK.

*These authors contributed equally to this work.
†To whom correspondence should be addressed. E-mail: philippe.bastiaens@embl-heidelberg.de

body binding are rate-limiting, and steric hindrance after antibody binding can slow the phosphorylation reaction. To properly capture the initial phosphorylation in the proximity of the bead and the subsequent propagation across the plasma membrane, cells were stimulated with Cy5-labeled EGF-beads for short periods (10 to 60 s) and immediately fixed and incubated with Cy3/PY72 antibody. By controlled manipulation, we were able to retain the majority of the ErbB1-bound EGF-beads at their original location, as verified by microscopy. Indeed, soon after stimulation (10 to 30 s), phosphorylated ErbB1 was found in a patch containing the EGF-bead, clearly demonstrating lateral spreading of receptor activation originating from the point of stimulation (Fig. 2B). At 60 s, a homogenous activation pattern encompassing the whole plasma membrane was observed, demonstrating that lateral signal spreading is a rapid process.

To determine the evolution of ErbB1 phosphorylation precisely in time, a comparison between responses to stimulation with soluble EGF (Fig. 3A) and EGF-beads (Fig. 3B) was performed on large sets of cells. Soon after exposure, the cells stimulated with soluble EGF already showed a homogenous phosphorylation pattern as opposed to the patches of phosphorylated receptor found after EGF-bead stimulation (Fig. 3, A and B). Later, the extent of ErbB1 phosphorylation for both focal and homogenous stimulation was indistinguishable. Receptor internalization was observed within the whole cell after 20 to 30 min for both types of stimuli, thus providing independent evidence for the existence of activated receptors not bound to EGF ligand. This occurrence of endocytosis was also confirmed by confocal microscopy of ErbB1-GFP in live MCF7 cells stimulated with Cy3-labeled EGF-beads, clearly showing the uptake of vesicular structures inside the cell. For both stimulation conditions, plasma membrane populations of phosphorylated receptor locally approached 100%.

Generally, lower population sizes of phosphorylated receptor were found in the center of the cell because of the presence of ErbB1-GFP that was not exposed to the extracellular stimulus; either de novo receptor in transit to the plasma membrane, or receptors participating in endocytosis before stimulation. The average populations of phosphorylated ErbB1 for EGF and EGF-bead stimulation for each

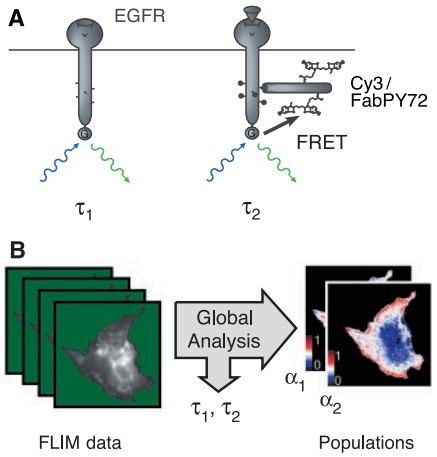

Fig. 1. Quantitative imaging of ErbB1 phosphorylation using FLIM coupled with global analysis techniques. (**A**) FRET between the GFP on ErbB1 and Cy3 on antibodies to phosphotyrosine can be detected through a shortening of the GFP fluorescence lifetime (τ) measured by FLIM (*11*–*13*). Efficient FRET will only occur when the Cy3 acceptor is brought within nanometer range of the GFP donor by binding of the antibody to the phosphorylated receptor. The high signal specificity of these binding events arises from the measurement of FRET through the donor lifetime exclusively, even when the acceptor-carrying antibody is not specific for its epitope or present in excess (*11*), enabling the use of generic antibodies to phosphotyrosine. Two receptor states, bound and unbound to antibody, exist at every spatially resolvable image element (pixel), each associated with a unique spatially invariant fluorescence lifetime corresponding to the presence (τ_2) or absence (τ_1) of FRET. However, the parameters of interest are the populations of the two protein states in each pixel. (**B**) Global analysis (*33*) of FLIM data (*18*) uses the understanding that only two protein states, with their spatially invariant fluorescence lifetimes are present in each pixel. All pixels are simultaneously analyzed giving the two lifetimes and the population maps (α_1 and α_2) that show the relative concentrations of molecules in each state. The true FRET efficiency in the protein complex (E_c) is calculated by $E_c = 1 - \tau_2/\tau_1$. Global analysis can be applied to large collections of sets, thereby greatly improving accuracy and precision. From an error analysis, we calculated that the errors of the populations in each pixel ranged from 5 to 10%.

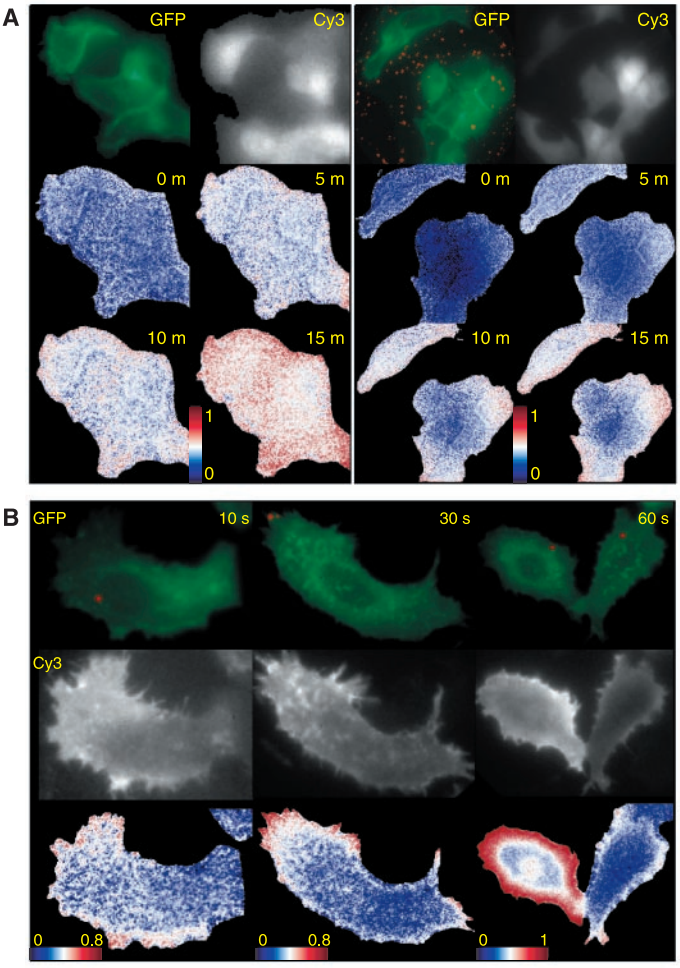

Fig. 2. Phosphorylation of ErbB1-GFP in response to EGF-bead stimulation. (**A**) Populations of phosphorylated ErbB1-GFP receptors in live cells. MCF7 cells growing on glass-bottom culture dishes were starved in Dulbecco's modified Eagle's medium (DMEM) containing 0.5% serum for 5 hours before transfer to phenol red and riboflavin-free, low-bicarbonate DMEM medium supplemented with 25 mM Hepes, pH 7.4, before microinjection with Cy3/FabPY72. Left panel, stimulation with EGF (in minutes); right panel, stimulation with EGF-beads (red dots, top left panel). Top panels, ErbB1-GFP and Cy3/FabPY72 fluorescence intensity images; lower panels, images of the ErbB1-GFP phosphorylation state. Color bars represent population values. A single global analysis of all FLIM data sets ($n = 12$) yielded fluorescence lifetimes of $\tau_1 = 2.2$ ns and $\tau_2 = 0.56$ ns ($E_c = 75\%$). (**B**) Correlation between phosphorylated ErbB1-GFP and the position of EGF-beads (red dots, top row). Cells were fixed with 4% formaldehyde after incubation with Cy5-labeled EGF-beads on the indicated time points to capture the initial phosphorylation wave. Permeabilization and incubation with antibody were performed under controlled conditions that maintain the position of the bead throughout the procedure as verified by microscopic observation. Top row, ErbB1-GFP fluorescence intensity (green) overlaid with Cy5-labeled EGF-bead fluorescence (red); middle row, Cy3/PY72 fluorescence intensity images; bottom row, Population of phosphorylated ErbB1-GFP receptors. Color bars represent population values. A single global analysis of all FLIM data sets ($n = 55$) yielded fluorescence lifetimes of $\tau_1 = 2.4$ ns and $\tau_2 = 0.94$ ns ($E_c = 61\%$).

time point are shown in Fig. 3C, computed in each case from a global analysis of the FLIM measurements of several hundred cells. Soon after stimulation (<1 min), the average population of phosphorylated receptors is significantly lower for bead-stimulated cells because of the presence of phosphorylated receptor in patches. After a 1-min incubation with EGF or EGF-beads, the average populations of phosphorylated receptors are indistinguishable and reach the maximal level. These populations then decrease over longer stimulation periods because of shielding of the phosphorylated tyrosine residues by recruitment of proteins to internalized ErbB1-GFP (*13*).

Spreading of phosphorylation after focal stimulation implies dissociation of activated receptors from dimers and subsequent activation of receptors without ligands located outside the area stimulated by the EGF-bead. Fluorescence recovery after photobleaching (FRP) was performed to exclude the possibility of ligand-induced spreading of ErbB1 phosphorylation by diffusion and exchange with bead-bound receptors. The high GFP fluorescence intensity observed around the bead did not reappear after photobleaching, showing that receptors underneath the bead are tightly bound and do not exchange on the time scale in which spreading of phosphorylation is observed (Fig. 4). In addition, diffusion of the ErbB1 receptors as calculated from FRP data (legend to Fig. 4) was considerably slower

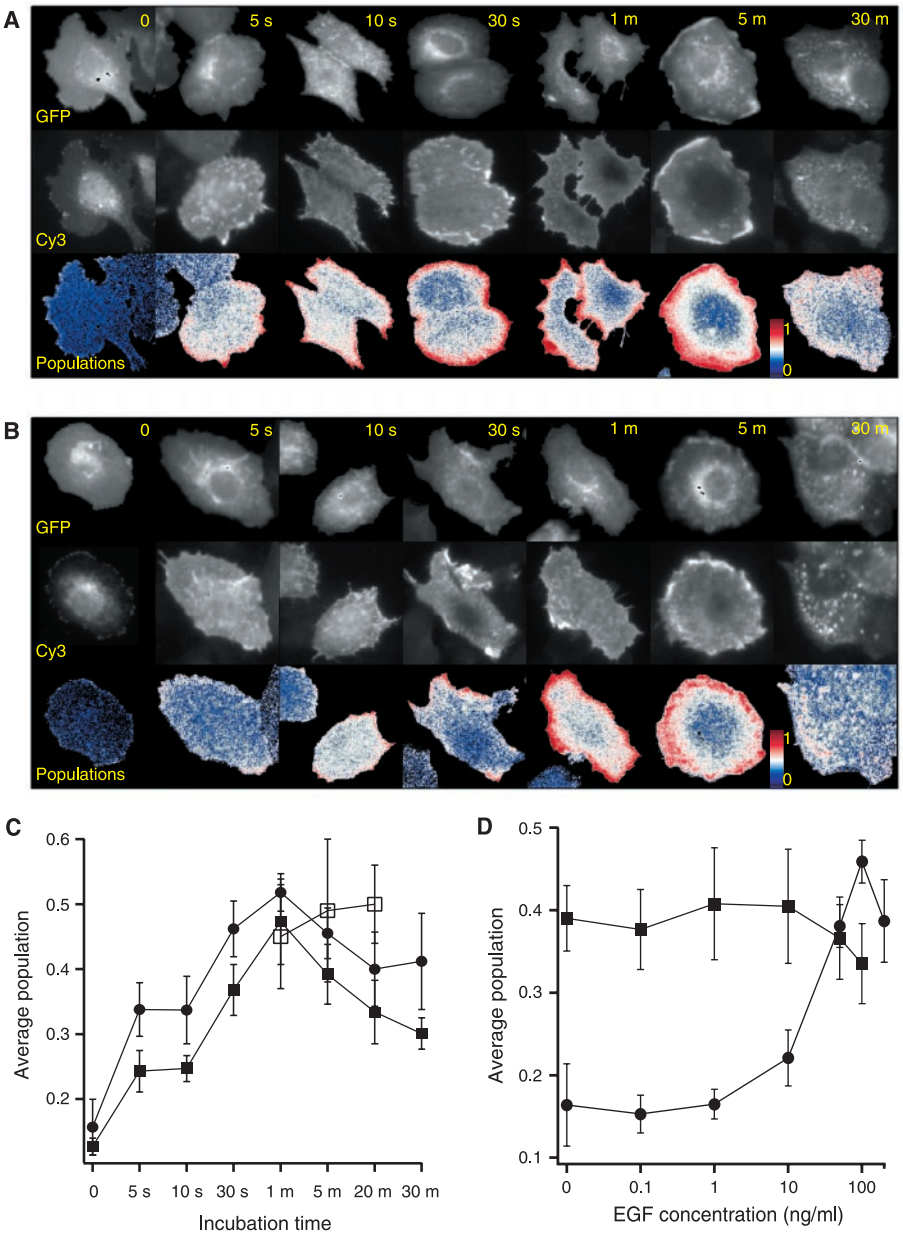

Fig. 3. Time course of phosphorylation of ErbB1-GFP receptors in MCF7 cells stimulated with EGF and EGF-beads. Fixation and antibody incubation were performed as described previously (*13*). (**A**) Populations of phosphorylated ErbB1-GFP receptors after stimulation with EGF. A single global analysis of all FLIM data sets (n = 97) returned fluorescence lifetimes of τ_1 = 2.2 ns and τ_2 = 0.84 ns (E_c = 62%). A single representative cell is shown out of a set of 10 measurements for each time point. Top panels, ErbB1-GFP fluorescence intensity; middle panels, Cy3/PY72 fluorescence intensity; lower panels, populations of phosphorylated receptor. Color bar represents population values. (**B**) Populations of phosphorylated ErbB1-GFP after local stimulation with EGF-beads. A single global calculation of all FLIM data sets (n = 81) yielded fluorescence lifetimes of τ_1 = 2.2 ns and τ_2 = 0.83 ns (E_c = 62%). (**C**) Average population of phosphorylated ErbB1-GFP receptors plotted as a function of incubation time with soluble EGF (filled circles) or EGF-beads (filled squares). Also plotted are average populations of phosphorylated ErbB1-GFP receptors in EGF-bead–stimulated MCF7 cells incubated with the Src family kinase inhibitor PP2 (open squares). (**D**) EGF dose-response curve of ErbB1-GFP receptor phosphorylation. The average populations of phosphorylated ErbB1-GFP in the absence (circles) and presence (squares) of 1 μM phosphatase inhibitor PAO is plotted as a function of EGF concentration.

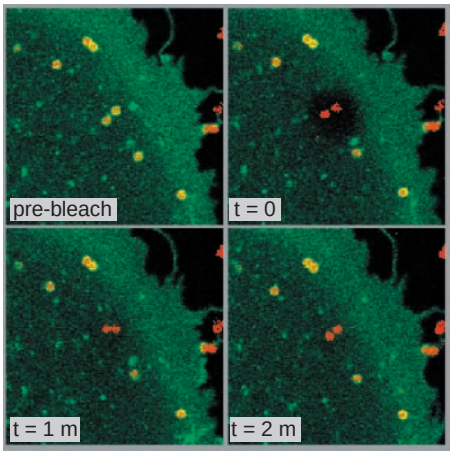

Fig. 4. FRP experiments. Cells incubated for 10 min with Cy3-labeled EGF-beads were imaged with a Zeiss LSM 510 confocal microscope. A region of interest was photobleached with a 488-nm argon laser at full power. Fluorescence recovery was monitored at 2-s intervals using a 488-nm argon laser (GFP channel, LP505 emission filter) and a 543-nm HeNe laser (Cy3 channel, LP530 emission filter). Shown are red/green overlays of the intensities of ErbB1-GFP (green) and Cy3-labeled EGF-beads (red) for four images out of a series of 120 (2-s interval). Before GFP photobleaching of a circular region (2.3-μm radius), the intensities of all beads on the cell strongly correlated to those of ErbB1-GFP (yellow dots), indicating a high quantity of ErbB1-GFP receptors binding to the EGF-beads. After photobleaching, only the Cy3 signal (red) remained on the beads in the bleached region. At 1 min, most ErbB1-GFP fluorescence has recovered by diffusion, except at the bead positions, showing that the photobleached ErbB1-GFP is bound to the bead. The diffusion constant of ErbB1-GFP in the plasma membrane was 0.032 ± 0.010 $\mu m^2/s$, calculated from 10 independent experiments with the method described in (*34*).

than the lateral signal propagation. The relative immobility of the beads observed in these measurements also precludes large-scale movements of the beads as a cause for extended distribution of phosphorylated ErbB1.

Independent evidence that dissociation of activated receptors induces lateral spreading of phosphorylation was obtained by using intrinsically kinase-dead (*23*) ErbB3-GFP (*24*) cotransfected with ErbB1 at low ErbB1-to-ErbB3-GFP expression ratios. When dimers are indeed a transient feature, activated ErbB1 receptors should be able to phosphorylate multiple neighboring ErbB3-GFP receptors that, on their own, are not able to propagate the signal, and the proportion of phosphorylated ErbB3-GFP receptors should exceed that of ErbB1. An average population of 43 ± 8% (n = 13 cells) phosphorylated ErbB3-GFP was found when the expression ratio of ErbB1 to ErbB3-GFP was 1:10, after a 5-min incubation with 0.1 μg/ml EGF. This is significantly more than the fraction of ErbB1 receptors (10%), strongly corroborating transient dimerization as a key feature of the propagation of phosphorylation.

Control cells expressing only ErbB3-GFP did not show EGF-induced phosphorylation. To exclude inside-out signaling by a cytosolic tyrosine kinase instead of ErbB1 transphosphorylation, two additional experiments were performed. Cells were permeabilized with streptolysin O (*25*), to remove soluble protein from the cytosol before stimulation (5 min) with EGF or EGF-beads. The same whole-cell activation pattern was observed, showing that no soluble protein factor is involved in the lateral signaling process. Also, to exclude the involvement of Src-type tyrosine kinases in the ErbB1 transphosphorylation process, the cells were also stimulated with EGF-beads after incubation with 50 nM of PP2, an inhibitor of the SRC family kinases (Calbiochem, San Diego, California). Again, full and extended phosphorylation of ErbB1-GFP in the plasma membrane was seen (Fig. 3C). Owing to inhibition of Src-type kinases by PP2, delayed internalization of ErbB1 was observed (*26*), which resulted in sustained measured phosphorylation levels (*13*) (Fig. 3C).

To investigate the role of receptor tyrosine phosphatases (*27*) in ErbB1 lateral signaling, we compared average ErbB1 phosphorylation levels at different EGF concentrations in the presence and absence of the phosphatase inhibitor phenylarsine oxide (PAO, Sigma). The steep dependence of receptor phosphorylation on EGF concentration was lost after addition of PAO, resulting in maximal ErbB1 activation (Fig. 3D). These results indicate that ErbB1 kinase activity is suppressed by phosphatase activity in resting cells that must be overcome to initiate lateral signal propagation.

Evidence of ErbB1 dimerization as a mechanism of activation has been provided in the past by in vivo cross-linking experiments (*4*, *28*, *29*). In these studies, only a minor fraction of ErbB1 receptors was separated as dimers by gel electrophoresis, which was explained by inefficient cross-linking. In our view, this observed dimer band was minor owing to the small steady-state population of transient dimers in the lateral signaling process after growth factor stimulation. Lateral ErbB1 signaling is also supported by previous immunoprecipitation studies on cells coexpressing different ErbB family members. Paradoxical ErbB1-ErbB2 dimers were detected after stimulation with the ErbB3/ErbB4 ligand heregulin (HRG) and ErbB2-ErbB3/ErbB4 dimers after stimulation with the ErbB1-ligand EGF (*30*, *31*).

These findings also corroborate an activation mechanism involving transient rather than stable receptor dimers. Signal propagation at the plasma membrane provides an early amplification mechanism, preceding that in the extensively investigated axial direction. This mechanism will spread the signal of localized ErbB stimulation events, for example, in the case of cell-cell contact between ErbB1-bearing cells and cells exposing membrane-bound ligands (pre-EGF, pre–transforming growth factor–α or heparin-bound EGF).

The existence of this mode of ErbB1 receptor activation further implies that local threshold concentrations of growth factors can fully activate ErbB1-linked growth regulatory signal cascades. This threshold is set for each cell individually by its specific intrinsic phosphatase activity. A possible initiation mechanism for ErbB1 activation is that ligand-induced receptor aggregation locally increases the kinase activity sufficiently to overcome phosphatase action. Lateral signal propagation then proceeds via a phosphorylation-induced increase in kinase activity of ErbB1 or by phosphorylation-dependent inhibition of phosphatases. In either case, the cell is committed to a phosphorylation cascade that is no longer dependent on growth factor. As the ErbB growth factor receptor family has been implicated in the development and progression of human cancers (*32*), lateral signal transduction might represent an attractive target for pharmacological intervention of malignant ErbB activation at an early and accessible stage in the signaling process.

References and Notes

1. A. Weiss, J. Schlessinger, *Cell* **94**, 277 (1998).
2. M. Mohammadi *et al.*, *Biochemistry* **32**, 8742 (1993).
3. Y. Yarden, J. Schlessinger, *Biochemistry* **26**, 1443 (1987).
4. C. Cochet *et al.*, *J. Biol. Chem.* **263**, 3290 (1988).
5. M. Zhou *et al.*, *Biochemistry* **32**, 8193 (1993).
6. Y. Yarden, J. Schlessinger, *Biochemistry* **26**, 1434 (1987).
7. A. M. Honegger, R. M. Kris, A. Ullrich, J. Schlessinger, *Proc. Natl. Acad. Sci. U.S.A.* **86**, 925 (1989).
8. I. Alroy, Y. Yarden, *FEBS Lett.* **410**, 83 (1997).
9. T. Pawson, *Oncogene* **3**, 491 (1988).
10. W. M. Kavanaugh, L. T. Williams, *Science* **266**, 1862 (1994).
11. P. I. H. Bastiaens, A. Squire, *Trends Cell Biol.* **9**, 48 (1999).
12. T. Ng *et al.*, *Science* **283**, 2085 (1999).
13. F. S. Wouters, P. I. H. Bastiaens, *Curr. Biol.* **9**, 1127 (1999).
14. A. Squire, P. I. H. Bastiaens, *J. Microsc.* **193**, 36 (1999).
15. J. R. Lakowicz, K. Berndt, *Rev. Sci. Instrum.* **62**, 1727 (1991).
16. T. W. J. J. Gadella, T. M. Jovin, R. M. Clegg, *Biophys. Chem.* **48**, 221 (1993).
17. Images were taken with a Zeiss plan-Apochromat 100X/1.4 NA PH3 oil objective at a modulation frequency of 80 MHz. GFP was excited by using a 488-nm Argon laser line, and the fluorescence was detected using a dichroic beamsplitter (Q 505 LP; Chroma Technology Corp., Brattleboro, VT) and a narrow-band emission filter (BP514/10; Lys & Optik). Cy3 images were recorded using a 100 W Mercury arc lamp (Zeiss Attoarc) with a high Q Cy3 filter set (exciter:HQ, 535/50; dichroic:Q, 565 LP; emitter:HQ, 610/75 LP; Chroma Technology Corp.). Live cell imaging was performed at 37°C.
18. P. J. Verveer, A. Squire, P. I. H. Bastiaens, *Biophys. J.* **78**, 2127 (2000).
19. Y. Nagai *et al.*, *Nature Biotechnol.* **18**, 313 (2000).
20. Carboxyl-modified polystyrene beads (Sigma) were incubated for 15 min in 50 mM MES, pH 6.1, supplemented with 2 mM 1-ethyl-3-(3-dimethylaminopropyl)carbodiimide-HCL (EDAC) and 5 mM N-hydroxysuccinimide (NHS) at room temperature. The reaction was stopped with 20 mM 2-mercaptoethanol and washing with MES buffer. The beads were reacted with EGF in MES buffer (at 10 μg/μl dry beads) for 2 hours at room temperature, followed by 15 hours at 4°C. Beads were quenched for 15 min in 10 mM hydroxylamine and washed with phosphate-buffered saline. Approximately 10^5 EGF molecules were bound per bead. For stimulation times up to 1 min, coverslips with cells were drained and overlaid with 25 μl (4×10^5 beads per microliter) suspension. For longer stimulation times, 25 μl (2×10^5 beads per microliter) suspension was added to coverslips in 24-well culture dishes (0.25 ml medium) amounting to 2 to 5 beads per cell.
21. Supplementary material is available to *Science* Online subscribers www.sciencemag.org/cgi/content/full/290/5496/1567/DC1.
22. F. S. Wouters, P. I. H. Bastiaens, in *Current Protocols in Cell Biology*, J. S. Bonifacino, M. Dasso, J. Lippincott-Schwartz, J. B. Harford, K. M. Yamada, Eds. (Wiley, New York, 2000), vol. 17.1, pp. 17.1.1–17.1.15.
23. P. M. Guy, J. V. Platko, L. C. Cantley, R. A. Cerione, K. L. Carraway III, *Proc. Natl. Acad. Sci. U.S.A.* **91**, 8132 (1994).
24. Constructed similarly to ErbB1-GFP (*13*).
25. L. Buday, J. Downward, *Mol. Cell. Biol.* **13**, 1903 (1993).
26. A. Wilde *et al.*, *Cell* **96**, 677 (1999).
27. F. U. Weiss, H. Daub, A. Ullrich, *Curr. Opin. Genet. Dev.* **7**, 80 (1997).
28. O. Kashles, Y. Yarden, R. Fischer, A. Ullrich, J. Schlessinger, *Mol. Cell. Biol.* **11**, 1454 (1991).
29. A. Sorokin, M. A. Lemmon, A. Ullrich, J. Schlessinger, *J. Biol. Chem.* **269**, 9752 (1994).
30. M. M. Marques, N. Martinez, I. Rodriguez-Garcia, A. Alonso, *Exp. Cell. Res.* **252**, 432 (1999).
31. D. C. Gamett, G. Pearson, R. A. Cerione, I. Friedberg, *J. Biol. Chem.* **272**, 12052 (1997).
32. D. S. Salomon, R. Brandt, F. Ciardiello, N. Normanno, *Crit. Rev. Oncol. Hematol.* **19**, 183 (1995).
33. J. M. Beechem, *Methods Enzymol.* **210**, 37 (1992).
34. D. M. Soumpasis, *Biophys. J.* **41**, 95 (1983).

35. ErbB1 in pcDNA3.1 was a gift from C. Dickson (Imperial Cancer Research Fund, London). P.J.V. and F.S.W. were supported by long-term fellowships from the European Molecular Biology Organization. We thank E. Karsenti and A. Squire at EMBL for critically reading the manuscript and making useful suggestions.

11 September 2000; accepted 12 October 2000